Virology 388 (2009) 324–334

Contents lists available at ScienceDirect

Virology

journal homepage: www.elsevier.com/locate/yviro

Two adjacent mutations on the dimer interface of SARS coronavirus 3C-like protease cause different conformational changes in crystal structure☆

Tiancen Hu [a,1], Yu Zhang [a,1], Lianwei Li [a], Kuifeng Wang [a], Shuai Chen [a], Jing Chen [a], Jianping Ding [b], Hualiang Jiang [a,*], Xu Shen [a,*]

[a] Drug Discovery and Design Center, State Key Laboratory of Drug Research, Shanghai Institute of Materia Medica, Chinese Academy of Sciences, 555 Zuchongzhi Road, Pudong, Shanghai 201203, China
[b] State Key Laboratory of Molecular Biology, Institute of Biochemistry and Cell Biology, Shanghai Institutes for Biological Sciences, Chinese Academy of Sciences, 320 Yueyang Road, Shanghai 200031, China

ARTICLE INFO

Article history:
Received 6 February 2009
Returned to author for revision
6 March 2009
Accepted 30 March 2009

Keywords:
SARS coronavirus
3C-like protease
Dimerization
Enzymatic activity
Mutation
Monomer

ABSTRACT

The 3C-like protease of SARS coronavirus (SARS-CoV 3CL^{pro}) is vital for SARS-CoV replication and is a promising drug target. It has been extensively proved that only the dimeric enzyme is active. Here we discovered that two adjacent mutations (Ser139_Ala and Phe140_Ala) on the dimer interface resulted in completely different crystal structures of the enzyme, demonstrating the distinct roles of these two residues in maintaining the active conformation of SARS-CoV 3CL^{pro}. S139A is a monomer that is structurally similar to the two reported monomers G11A and R298A. However, this mutant still retains a small fraction of dimer in solution, which might account for its remaining activity. F140A is a dimer with the most collapsed active pocket discovered so far, well-reflecting the stabilizing role of this residue. Moreover, a plausible dimerization mechanism was also deduced from structural analysis. Our work is expected to provide insight on the dimerization–function relationship of SARS-CoV 3CL^{pro}.

Introduction

Severe acute respiratory syndrome (SARS) (Stockman et al., 2006) is a highly infectious disease that broke out from November 2002 to July 2003, and it caused a lot of infection cases and deaths (Stockman et al., 2006). SARS coronavirus (SARS-CoV) is responsible for SARS disease (Drosten et al., 2003a, 2003b; Fouchier et al., 2004; Ksiazek et al., 2003; Peiris et al., 2003). The genome of SARS-CoV contains 14 functional open reading frames (ORFs) (Thiel et al., 2003). The two large 5′-terminal ORFs, 1a and 1b encode two overlapping polyproteins, pp1a and pp1ab, which have to be cleaved extensively to produce proteins necessary for viral RNA synthesis and genome replication (Anand et al., 2003; Thiel et al., 2003; Ziebuhr et al., 2000). Such proteolytic processing is performed by two viral proteases, the papain-like cysteine protease (PL2^{pro}) and the chymotrypsin-like protease called 3C-like protease (3CL^{pro}) due to its distant relationship with the 3C proteases of picornaviruses (Ziebuhr et al., 2000). While PL2^{pro} has extra functions like deubiquitination (Barretto et al., 2005, 2006; Lindner et al., 2005, 2007; Ratia et al., 2006; Sulea et al., 2005) and antagonizing type I interferon to counteract innate immunity (Devaraj et al., 2007), 3CL^{pro} plays a major role in processing viral polyproteins and controlling the activities of replication complexes, thus is also called the main protease (M^{pro}). Meanwhile, it has been also shown to induce mitochondrial-mediated apoptosis (Lai et al., 2007; Lin et al., 2006). Therefore, for its functional indispensability in viral life cycle, SARS-CoV 3CL^{pro} has become an attractive target for discovering new anti-SARS agents.

In crystal structure, SARS-CoV 3CL^{pro} forms a dimer with two monomers oriented perpendicular to one another (Yang et al., 2003), similar to the TGEV and HCoV 3CL^{pro} structures (Anand et al., 2002, 2003), in which each monomer contains three domains. Domains I and II (residues 8–101 and residues 102–184) each fold into an antiparallel β-barrel and together form a chymotrypsin fold responsible for catalysis. The substrate-binding site is located in a cleft between these two domains. Domain III (residues 201–306) is a globular cluster of five antiparallel α-helices connected to the chymotrypsin fold by a long loop (residues 185–200) (Anand et al.,

Abbreviations: SARS-CoV, severe acute respiratory syndrome coronavirus; 3CL^{pro}, 3C-like protease; RMSD, root-mean-square deviation; MES, 2-(N-morpholino)ethanesulfonic acid; PEG, polyethylene glycol; DTT, dithiothreitol; DMSO, dimethyl sulphoxide; EDTA, ethylene diaminetetraacetic acid; IPTG, isopropyl β-D-thiogalactoside.

☆ Coordinates and structure factors of the two SARS-CoV 3CL^{pro} mutants have been deposited in the Protein Data Bank with accession number of 3F9E for S139A, and 3F9F, 3F9G, and 3F9H for F140A.

* Corresponding authors. Fax: +86 21 50806918.
E-mail addresses: hljiang@mail.shcnc.ac.cn (H. Jiang), xshen@mail.shcnc.ac.cn (X. Shen).

[1] These two authors contributed equally to this work.

0042-6822/$ – see front matter © 2009 Elsevier Inc. All rights reserved.
doi:10.1016/j.virol.2009.03.034

2002, 2003; Shi et al., 2004; Yang et al., 2003). It plays a major role in SARS-CoV 3CL^{pro} dimerization, reflecting one of the most intriguing properties of the enzyme.

SARS-CoV 3CL^{pro} exists in a equilibrium of dimer and monomer in solution (Chou et al., 2004; Fan et al., 2004; Graziano et al., 2006a, 2006b; Hsu et al., 2005a, 2005b), with a dissociation constant K_D lower than 100 nM (Hsu et al., 2005b; Kuo et al., 2004; Verschueren et al., 2008). Since it has been widely proved that only the dimer is active (Barrila et al., 2006; Chang et al., 2007; Chen et al., 2005, 2006, 2008b; Chou et al., 2004; Fan et al., 2004; Graziano et al., 2006b; Hsu et al., 2005b; Lin et al., 2008), the dimer interface is regarded as an ideal target for structure-based enzyme inhibitor design. The major components of the interface are: (i) the N-terminal residues 1–7 (N-finger), (ii) the S1 substrate-binding subsite, (iii) helix A′ (residues 10–15) that immediately follows the N-finger, and (iv) domain III. Fig. 1 illustrates the complete interaction network among these elements.

The S1 subsite confers the enzyme an absolute specificity for a glutamine at the P1 position of the substrate (Gln-P1). Moreover, it lies immediately next to the catalytic dyad (Cys145 and His41), and uses a structural element called the "oxyanion hole" to stabilize the tetrahedral intermediate produced during proteolysis (Fig. 1a). Thus, maintaining the intact conformation of S1 subsite is vital for catalysis, and this is exactly the major function of the counterpart N-finger (Fig. 1a). In brief, the Ser1B…Phe140 interaction helps the large aromatic ring of Phe140 insert into the S1 subsite to hold it open and active; the Ser1B…Glu166 hydrogen bond constrains the position of Glu166 to prevent it from blocking the entrance of the S1 subsite; the Ser1B…Ser139, Gly2B…Ser139 and the serial Arg298B…Met6B…Tyr126A…Phe140A interactions all make substantial contributions to dimer stability (Shi et al., 2008). In fact, an octapeptide interface inhibitor, designed according to the sequence of the N-finger, has been found to specifically inhibit the activity and dimerization of the protease (Ding et al., 2005).

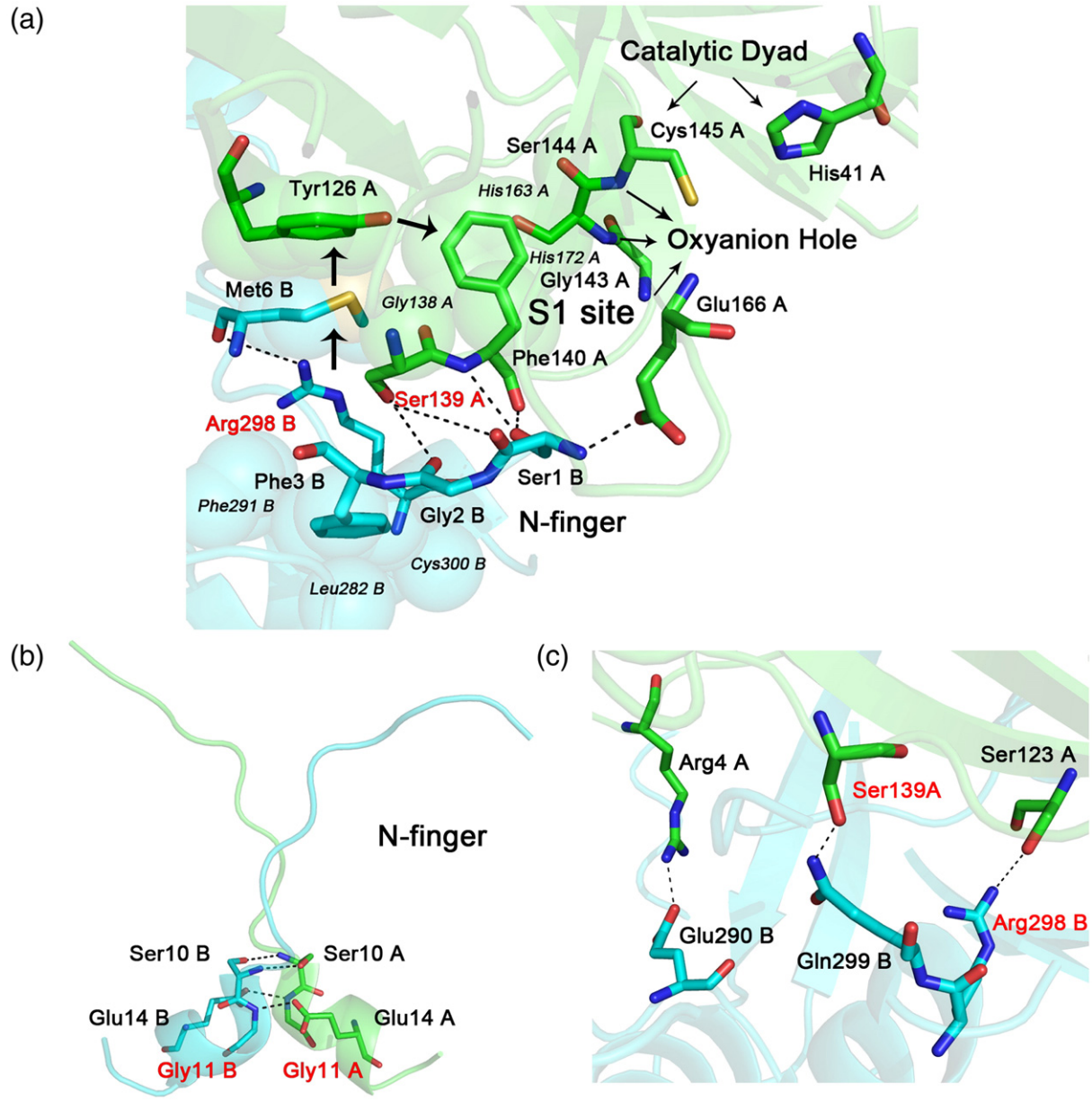

Fig. 1. The dimer interface of wild-type SARS-CoV 3CL^{pro} (PDB code: 1UK4). (a) The interactions between the S1 substrate-binding subsite from chain A (green) and the N-finger (cyan) from chain B. The dashes represent hydrogen bonds, and the spheres indicate hydrophobic interactions. The mutations of residues with red names have been proved to induce dimer dissociation of the enzyme. (b) The interactions between two helices A′. (c) The interactions between domain III from chain B and the N-finger and S1 subsite from chain A. (For interpretation of the references to colour in this figure legend, the reader is referred to the web version of this article.)

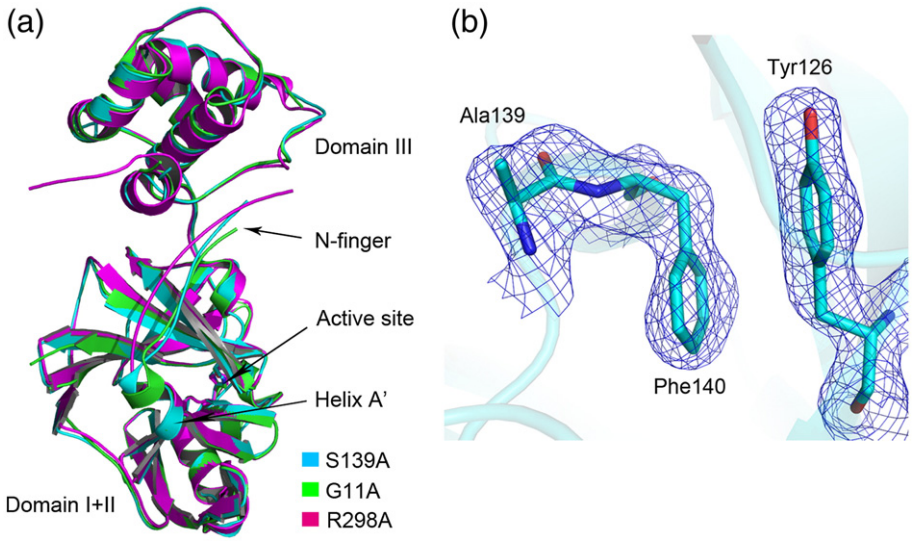

Fig. 2. (a) Overall structure of S139A mutant and its superposition with the other two structures of monomeric SARS-CoV 3CL^{pro} (G11A and R298A). The color scheme is indicated. (b) The $2F_o$–F_c electron density map contoured at 1.0σ around the mutated residue and two S1 subsite residues of S139A mutant. (For interpretation of the references to colour in this figure legend, the reader is referred to the web version of this article.)

Besides, the formation of H-bonds between the two helices A′ (Ser10A…Ser10B and Gly11A/B…Glu14B/A) is also the major stabilizer of the dimer interface (Fig. 1b). Actually the Gly11_Ala mutation has caused a crystallographic dissociation of SARS-CoV 3CL^{pro} dimer (Chen et al., 2008a). Last but not least, domain III has been extensively proved to be a key regulator of the dimerization and catalysis of SARS-CoV 3CL^{pro} (Anand et al., 2002; Bacha et al., 2004; Chang et al., 2007; Shi and Song, 2006; Shi et al., 2004; Ziebuhr et al., 1997). As shown in Figs. 1a and c, it not only directly contacts the opposite S1 subsite (Gln299B…Ser139, Arg298B…Ser123), but also helps position the N-finger properly to insert into the counterpart protomer by making both inter-protomer (Arg4B…Glu290) and intra-protomer (Arg298…Met6) interactions. As evidence, the Arg4B…Glu290 salt bridge has been demonstrated to be a key force in the dimerization of SARS-CoV 3CL^{pro} (Chou et al., 2004), and the Arg298_Ala mutation has produced yet another monomeric structure of the enzyme (Shi et al., 2008).

In order to evaluate the exact contributions of these interface residues to the dimerization and activity of SARS-CoV 3CL^{pro}, we previously conducted a systematic mutagenesis study of these residues combining biochemical, biophysical and crystallographic techniques (Chen et al., 2008a, 2008b). In the current work, we determined the crystal structures of two mutants S139A and F140A. Although S139A mutant is a monomer that is structurally similar to those of the other two reported monomers Gly11_Ala (Chen et al., 2008a) and Arg298_Ala (Shi et al., 2008), gel filtration analysis has clearly revealed the existence of the dimeric S139A in solution ascribing to its remaining enzymatic activity in solution. F140A, on the other hand, is still a dimer in crystal structure, with the dimer interface rearranged to some extent but at the cost of destructing the active site conformation. Its S1 subsite, especially the “oxyanion loop” has undergone the most dramatic conformational change ever reported at this site (Chen et al., 2008a; Shi et al., 2008; Yang et al., 2003), including a pH-dependent flip of the key substrate-binding residue His163, as revealed by three F140A structures at pH 6.0, 6.5 and 7.6. Together the structures of these two mutants suggested that the dimerization of SARS-CoV 3CL^{pro} is regulated by all the responsible elements in a cooperative manner, and its stability depends highly on the integrity of the dimer interface.

Results and discussion

Mutation choice

We chose to study the crystal structures of S139A and F140A mutants of SARS-CoV 3CL^{pro} mainly because of the following reasons. First, most of the reported mutant crystal structures are related to the mutations involved in the catalytic dyad (Hsu et al., 2005a), the helix A′ (Chen et al., 2008a) and domain III (Shi et al., 2008), which have provided profound insight into the dimerization-activity relationship of this enzyme. At the same time, the S1 substrate-binding subsite is another critical element involved in this issue, because it not only participates in catalysis but also directly contacts the opposite protomer. Thus, we selected the mutations of the two important residues Ser139 and Phe140 in this site. Second, these two mutations are adjacent to each other, but they exhibited completely different enzymatic activities (Chen et al., 2008b). It would be interesting to explore the underlying mechanism.

Crystal structure of S139A

Overall structure

To date, two crystal structures of monomeric SARS-CoV 3CL^{pro} have been reported, which are induced by mutations in helix A′ (Gly11_Ala) (Chen et al., 2008a) and domain III (Arg298_Ala) (Shi et al., 2008) respectively. The Gly11_Ala mutation caused the dimer dissociation by abolishing the entire interaction networks between the two opposing helices A′ (Fig. 1b), because (i) it interfered with the Gly11A/B…Glu14B/A interaction, and (ii) shortened helix A′ from residues 10–15 to 11–14, thus affecting the position of Ser10 and abolishing Ser10A/B…Ser10B/A H-bonds. As for Arg298_Ala, this mutation induced monomerization by disrupting the Arg298B…Ser123A H-bond and the serial interaction chain Arg298B…Met6B…Tyr126A…Phe140. In the current work, we discovered another

Fig. 3. Stereo illustrations and structural comparisons of the S1 subsite in S139A mutant. (a) The S1 subsite in the structure of the wild-type SARS-CoV 3CL^{pro} complexed with the substrate analog (chain A and G of the PDB entry 1UK4). Protein residues are colored in yellow, and the glutamine at the P1 position of the substrate analog is colored in pink. (b) S1 subsite comparison between wild-type (yellow) and S139A (cyan). Mutation-induced conformational changes were indicated by curved arrows. (c) S1 subsite comparison among the three monomeric structures of SARS-CoV 3CL^{pro}: S139A (cyan), G11A (green) and R298A (magenta).

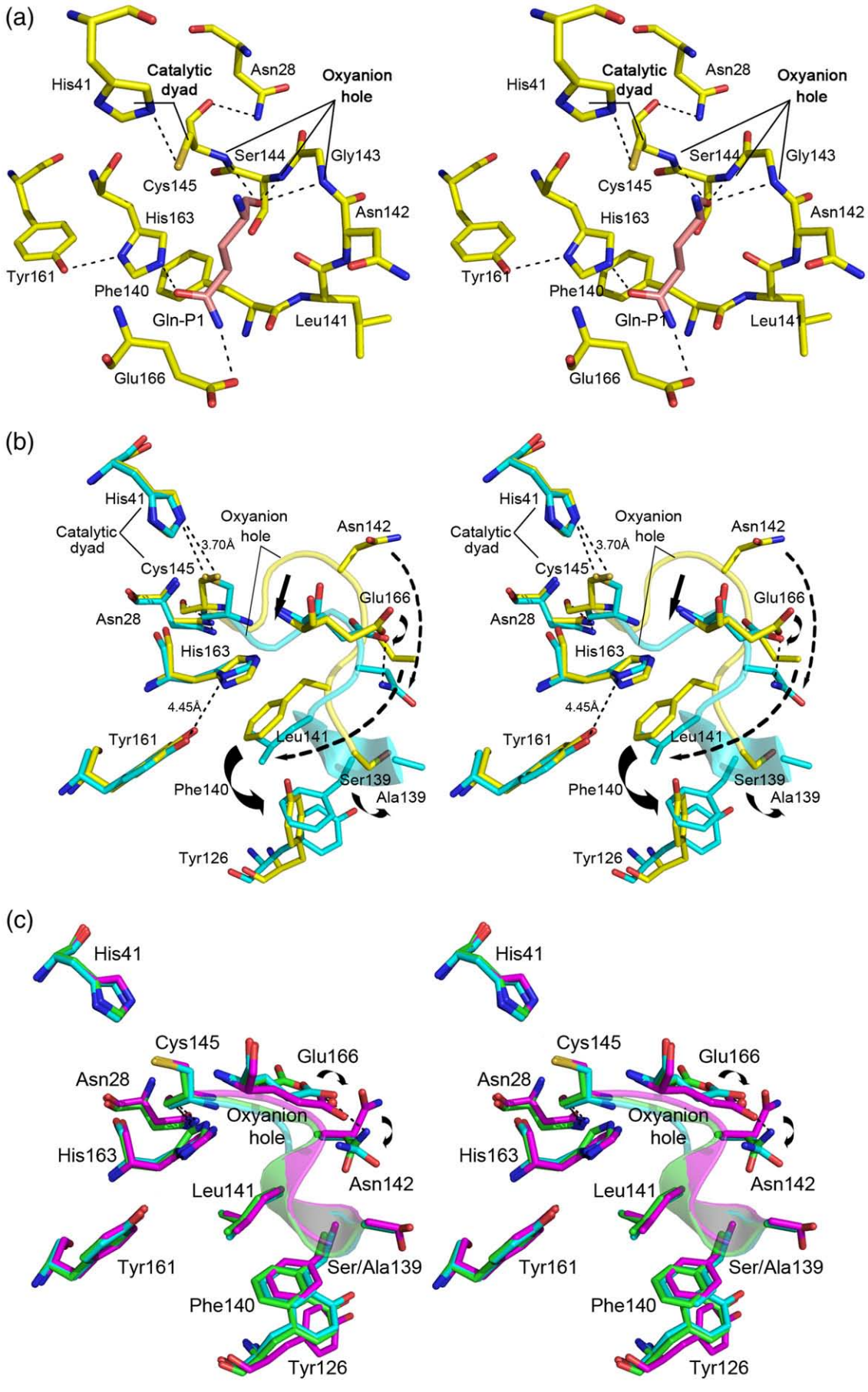
(a)
His41
Catalytic dyad
Asn28
Oxyanion hole
Ser144
Gly143
Cys145
His163
Asn142
Tyr161
Phe140
Gln-P1
Leu141
Glu166
(b)
His41
Catalytic dyad
Oxyanion hole
3.70Å
Asn142
Cys145
Glu166
Asn28
His163
4.45Å
Tyr161
Leu141
Ser139
Ala139
Phe140
Tyr126
(c)
His41
Cys145
Glu166
Asn28
Oxyanion hole
His163
Asn142
Leu141
Tyr161
Ser/Ala139
Phe140
Tyr126

monomeric crystal structure of SARS-CoV 3CL^{pro} by Ser139_Ala mutation. In the dimer structure, the sidechain hydroxyl of Ser139 forms hydrogen bonds with the mainchain carbonyls of Ser1B and Gly2B (Fig. 1a) as well as the sidechain amide of Gln299B (Fig. 1c). Thus, the mutation might have substantially destabilized the dimer interface. This again demonstrates that the integrity of the dimer interface is essential for dimerization, as supported by a lot of reports that a single mutation on the dimer interface could cause the complete dissociation of the dimer (Chen et al., 2008a; Hsu et al., 2005b; Lin et al., 2008; Shi et al., 2008; Shi and Song, 2006).

The overall structure of S139A is similar to those of G11A and R298A, with RMSD values being 0.40 Å and 0.69 Å, respectively (Fig. 2a). The $2F_o$–F_c electron density map clearly shows the mutation of Ser139 to alanine, as well as the flip of Phe140 from the S1 subsite toward Tyr126, which was also observed in G11A and R298A structures (Fig. 2b). The unique structural features associated with monomeric SARS-CoV 3CL^{pro}, namely the rotation of domain III and the "mis-orientation" of N-finger both exist in the S139A structure. The latter is especially worth noting. In our previous work with G11A, we thought the "mis-oriented" N-finger was caused by the mutation-induced shortening of helix A′ (Chen et al., 2008a). Now with the structures of R298A (Shi et al., 2008) and S139A, it is obvious that the mis-orientation of N-finger is an intrinsic property of monomeric SARS-CoV 3CL^{pro}. This observation could provide valuable clues for deducing the dimerization process of the enzyme. But to better understand this, we need to first inspect the structural changes of the active site.

Active site structure

As has been previously described about G11A and R298A structures, the catalytic dyad and the S1 subsite are the two key elements directly regulated by dimer–monomer switch of the enzyme. SARS-CoV 3CL^{pro} undergoes a general serine protease catalysis mechanism, and residues His41 and Cys145 have been identified as the catalytic dyad (Fig. 2a) (Huang et al., 2004). It was suggested that hydrogen bond formation between His41 NE2/ND1 and Cys145/SG could indicate the right conformation of the dyad (Chen et al., 2006). On the other hand, the substrate-binding pocket of SARS-CoV 3CL^{pro} is constituted by numerous subsites, S1′, S2′ and S1–S6, corresponding to the P1′, P2′ and P1–P6 residues on the peptide substrate. Among them, the S1 subsite is most important because its binding of a glutamine confers the enzyme absolute specificity for the Gln-P1 residue on the substrate. The S1 subsite could be divided into four parts: the oxyanion hole, His163, Glu166 and the various stabilizing elements (Fig. 2a). The oxyanion hole is constituted by the mainchain amides of Gly143, Ser144 and Cys145. An "open" oxyanion hole could not only recognize the mainchain oxygen of Gln-P1 but also stabilize the tetrahedral catalytic intermediate. This open conformation is supported by (i) Asn28…Gly143 interaction and (ii) the proper positioning of Phe140, which relies on its interaction with the opposite N-finger. The imidazole ring of His163 interacts with the sidechain oxygen of Gln-P1 and is held in place by (i) H-bond with the phenol hydroxyl of Tyr161 and (ii) stacking against the aromatic ring of Phe140, which also guarantees that this histidine remains uncharged over a wide range of pH values (Shi et al., 2008). The sidechain of Glu166 locates at the entrance of the pocket and recognizes the sidechain nitrogen of Gln-P1. It is constrained in an open state by H-bond with Ser1B from the opposite N-finger.

Fig. 3b shows the structural change of the active site in S139A monomer. Since some of the common features have been detailedly described in the study of G11A structure (Chen et al., 2008a), here we would only briefly point out the key changes. First, the distance between the two catalytic dyad residues increased to 3.70 Å, implying the catalytic dyad might be malfunctioning. Second, the oxyanion loop completely collapsed inward, as exemplified by the large movement of the sidechains of Asn142 and Leu141. In addition, the key supporting force Phe140 flipped away and packed with Tyr126 that adjusted its sidechain correspondingly. The position where Phe140 used to lie is now occupied by Leu141 to stack against His163. The stability of His163 was very likely to be undermined due to the disappearance of the Tyr161…His163 H-bond. Notably the sidechain of Glu166 directly formed an H-bond with the "slipped" Asn142 and blocked the entrance of the S1 subsite. This interaction was not observed in G11A and R298A monomer structures, suggesting the flexibility of the sidechains of Asn142 and Glu166 (Fig. 3c).

As has been indicated, the active site changes are basically similar for S139A, G11A and R298A structures (Fig. 3c), implying that these changes are stable conformations unique to the monomeric SARS-CoV 3CL^{pro}. Therefore, the support from the opposite protomer is essential for maintaining the correct conformation of the active site, but how does this interplay happen in the first place?

Implications for dimerization process

In our previous work about G11A mutant, we brought forward a plausible dimerization mechanism of SARS-CoV 3CL^{pro} based on the single monomer structure available at that time (Chen et al., 2008a). We thought that when two monomers approach each other, their domains III might initially form a dimer, then the two catalytic folds rotate to bring their N-fingers into each other and lock the dimer in a stable intermediate state. Finally the two domains III rotate to their final positions and further stabilize the dimer to form a mature and fully active enzyme. Now with the help of these three monomer structures (G11A (Chen et al., 2008a), R298A (Shi et al., 2008), and current work S139A), we could come up with a better conjecture about the dimerization process of SARS-CoV 3CL^{pro}, in which the movement of the N-finger could be better explained.

As mentioned before, the mis-oriented N-finger should actually be an intrinsic property of monomeric SARS-CoV 3CL^{pro}. But a question is also raised as to how the N-finger would change its position? We believe its movement is largely dependent on the rotation of domain III. After superposing the dimer and monomer structures based on their catalytic folds, we found that the positional relationship between domain III and the parental N-finger is actually unchanged in dimeric and monomeric enzymes (Fig. 4a). Further analysis revealed that their interaction patterns also remain similar in dimers and monomers (Figs. 4b and c). In detail, both Phe3 residues are wrapped by numerous hydrophobic residues including Trp207, Ala210, Leu282, Phe291 and Val296; and both Lys5 residues are salt-bridging to Glu290, the major stabilizing force of dimerization (Chou et al., 2004). Notably most of the interactions are mediated by regions around the last helix of domain III. Based on these observations, we thereby think it possible that these two important dimerization-related elements might actually be tethered together during the process of dimerization, which means that domain III might be the "motivator" controlling the movement of the N-finger.

Therefore, a possible dimerization process of SARS-CoV 3CL^{pro} might be supposed as follows. First, the trigger of the dimerization is very likely to be the association of two domains III, because domain III alone has been reported as stable dimers as well as monomers in solution (Shi et al., 2004; Zhong et al., 2008), while the catalytic fold alone cannot dimerize (Tan et al., 2005). It should be noted that the two domains III do not have any contact in the dimeric enzyme, thus their initial association should be temporary, presumably using the interface as reported recently (Zhong et al., 2008), just to bring two monomers close together. Subsequently, the catalytic folds might be close enough to anchor on each other, probably via the numerous H-bonds between the two helices A′. Based on this scaffold, the two domains III might dissociate and rotate themselves along with the tethered N-fingers to the opposite S1 subsites. In the last step, the Glu290…Arg4B salt bridge might help freeze the mature dimer (Chou et al., 2004), and Phe140…Ser1B, Ser139…Ser1B, Ser139…Gly2B

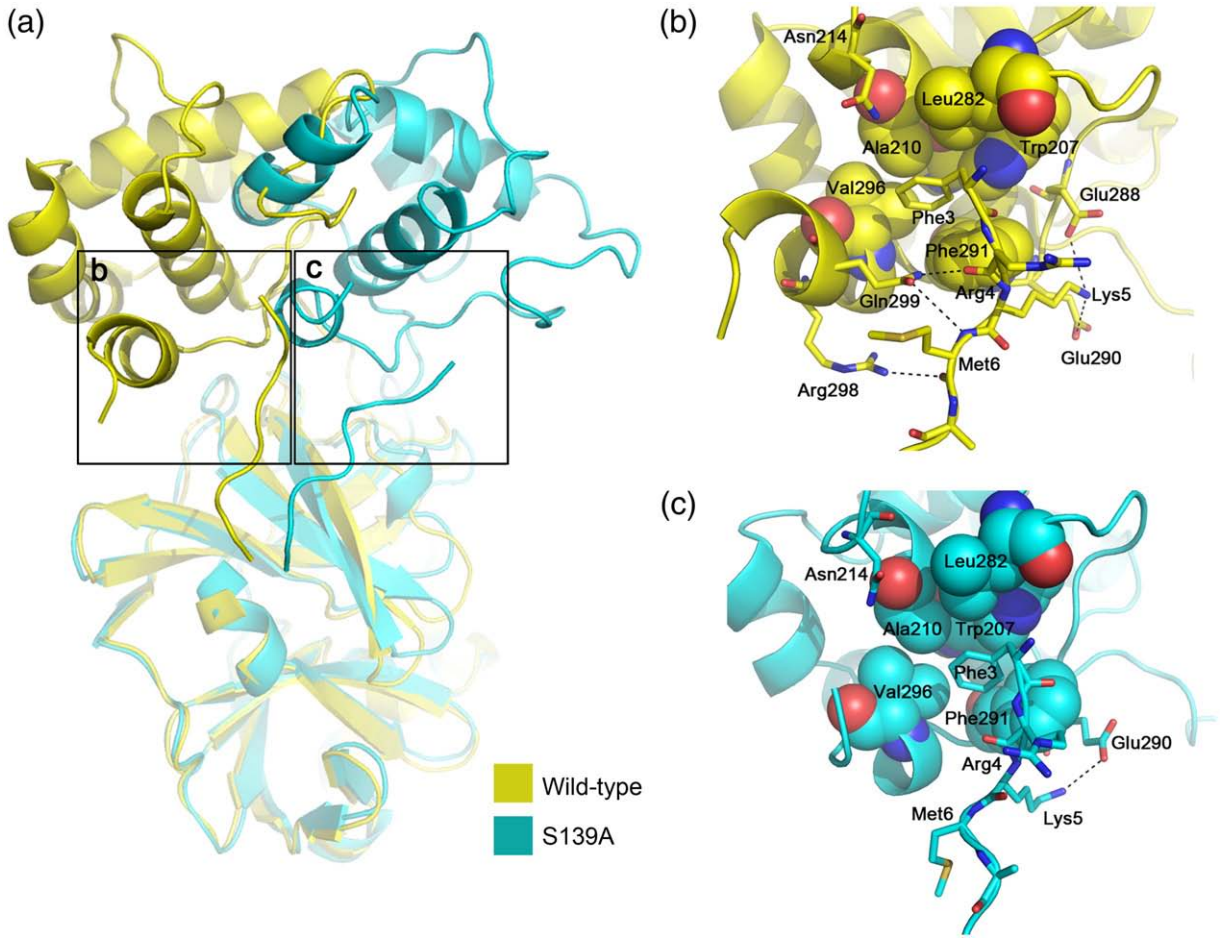

Fig. 4. Association between domain III and the parental N-finger. (a) The positional relationship between domain III and the parental N-finger remains similar in dimeric (yellow) and monomeric (cyan) SARS-CoV 3CL^{pro}. (b)(c) The detailed interactions between domain III and the parental N-finger. (For interpretation of the references to colour in this figure legend, the reader is referred to the web version of this article.)

interactions might directly activate the opposite S1 subsite. It also implies that these "activating" interactions might be the "result" rather than the "cause" of dimerization.

The reliability of this hypothesis could be supported by the findings that mutations in the key interactions involved in this dimerization process could severely impair the dimer stability of SARS-CoV 3CL^{pro} (Chen et al., 2008a; Hsu et al., 2005b; Lin et al., 2008; Shi et al., 2008; Shi and Song, 2006). These interactions include: (i) the initial association of the two domains III; (ii) the H-bonds between the two helices A′; (iii) the intra-protomer tethering between domain III and the N-finger; and (iv) the contact of domain III and the N-finger with the opposite S1 subsite. Remarkably, mutations and deletions in the last helix of domain III have caused great tendency of the enzyme to form monomers (Lin et al., 2008; Shi and Song, 2006). We believe this is at least partly due to the weakened affinity between domain III and the parental N-finger, which prevented domain III from efficiently bringing the N-finger to the opposite protomer during dimerization. This is supported by the fact that mutations of the first two N-terminal residues, which do not contact the parental domain III, have no obvious impact on SARS-CoV 3CL^{pro} activity (Chen et al., 2008b; Verschueren et al., 2008); while mutations beyond Phe3 in the N-finger caused drastic loss of the dimer stability and enzymatic activity (Chen et al., 2008b; Chou et al., 2004). As for the argument about whether the dimerization is triggered by the association of domain III (Zhong et al., 2008), a crystal structure of domain III alone might be highly desired to map the interface residues and direct the relevant mutagenesis confirmations.

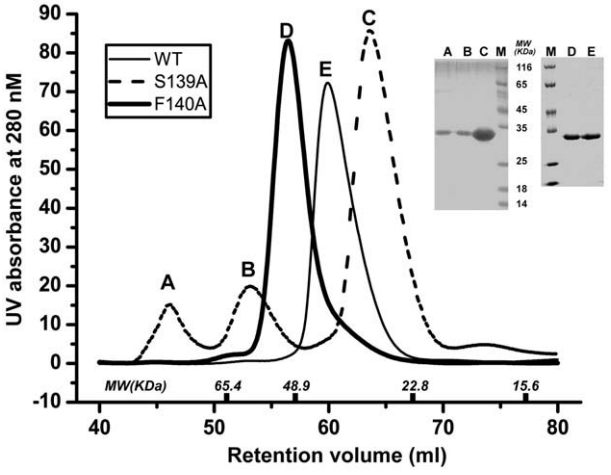

Fig. 5. Gel filtration analysis of SARS-CoV 3CL^{pro} S139A mutant. 2 mg/ml of the protein at neutral pH (7.5) was eluted on a HiLoad™ Superdex™ 75 prep grade column (GE Healthcare) at a flow rate of 1 ml/min. Marked on the *x*-axis are the molecular weight (MW) of the four marker proteins (namely ribonuclease A (15.6 kDa), chymotrypsinogen A (22.8 kDa), ovalbumin (48.9 kDa) and albumin (65.4 kDa)) at their specific retention volumes (Chen et al., 2005). The molecular weight of monomeric 3CL^{pro} is about 34 kDa. For S139A mutant, peak A and peak C represent stable dimer and monomer respectively, while peak B represents the equilibrium of monomer and dimer. Peak E and peak D represent wild-type and F140A mutant proteins respectively, which were both in the equilibrium of monomer and dimer. The contents of these peaks were all confirmed by SDS-PAGE (inset) to be SARS-CoV 3CL^{pro}.

The remaining activity of S139A

It is noticed that although S139A mutant is a monomer in crystal structure, it still retains some enzymatic activity in solution (Chen et al., 2008b). Gel filtration analysis of S139A showed that besides a majority of monomers, this mutant could still form a small fraction of stable dimer in solution (Fig. 5), which might be responsible for the remaining activity. As a control, the wild-type 3CL^{pro} migrated as a single peak in gel filtration chromatography (Fig. 5), representing an equilibrium between monomer and dimer, which was consistent with the previous report (Zhong et al., 2008). Therefore, it is possible that during the crystallization of S139A, only the more abundant and stable monomer form was incorporated into the crystal lattice.

Interestingly, the mutation of the adjacent residue Phe140 caused a contrary result. F140A is completely inactive yet remains a dimer in crystal. The reason underlying this difference will be described below.

Crystal structure of F140A

Overall structure

The crystal structure of F140A mutant is still a dimer. In addition, we managed to obtain three crystal structures of F140A at pH 6.0, 6.5 and 7.6, which could help find out whether pH variation would cause structural changes. All these F140A structures are very similar to that of the wild-type enzyme (PDB code: 1UK4), with RMSD values being 1.24 Å, 1.16 Å and 1.20 Å, respectively (Fig. 6a). The sidechain deletions of Phe140 could be clearly identified in the $2F_o$–F_c electron density maps (Fig. 6b).

Active site structure

In the wild-type structure, Phe140 is stabilized by interacting with Ser1B from the opposite protomer, and plays two major roles in maintaining the active state of the S1 subsite: (i) to uphold the open conformation of the oxyanion loop; and (ii) to stack against His163 and assure its uncharged state (Shi et al., 2008). Accordingly, the F140 mutation has caused damages on both aspects.

As shown in Fig. 6c, the oxyanion loops in the structures of F140A mutant all collapsed enormously inward. The movement of the oxyanion loops is about one-fold further than that observed in the monomer structure (Fig. 6c, the pink ribbon). The positions of Cys145 are also influenced by these large structural changes, increasing the distances between the catalytic dyad residues to 3.61 Å, 4.09 Å and 4.35 Å in structures at pH 6.0, 6.5 and 7.6, respectively, the latter two are among the largest ones observed in all known structures of SARS-CoV 3CL^{pro}. However, the sulfur atoms of Cys145 are still approximately in the plane of the His41 imidazole rings, as is in the wild-type structure.

As for the charging state of His163, we found an interesting phenomenon that the imidazole ring of His163 underwent a pH-dependent flip in the three structures, as obviously indicated in the

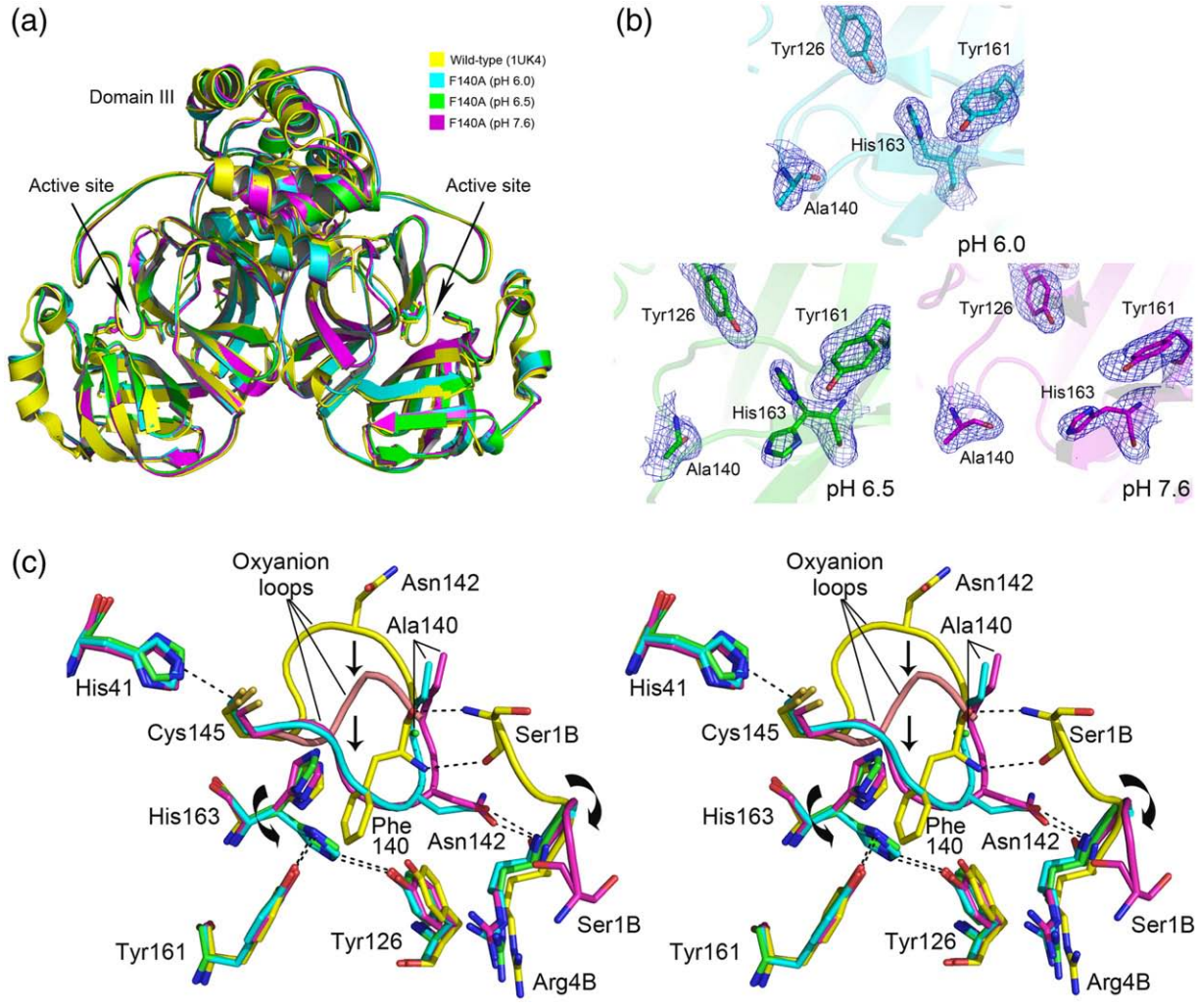

Fig. 6. Structural analysis of F140A mutant. (a) Superposition of three F140A structures determined at different pHs with the wild-type structure. The color scheme is indicated. (b) $2F_o$–F_c electron density maps contoured at 1.0σ around the mutated residues and some key S1 subsite residues. Note the different conformations of His163 at different pHs. (c) S1 subsite comparison among the wild-type structure (yellow), the S139A monomer structure (pink), and the three F140A structures. Note the large conformationals changes of the oxyanion loops in F140A, and the new Asn142…Arg4B interaction formed at the dimer interface.

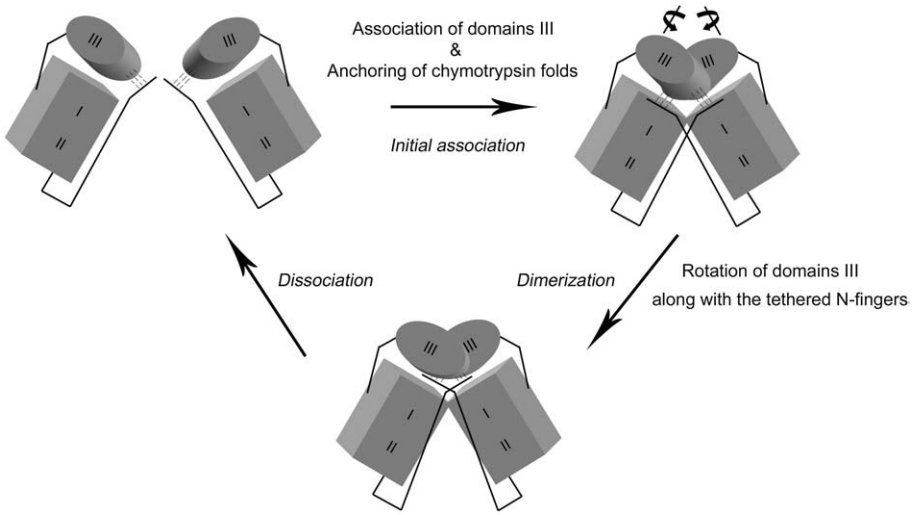

Fig. 7. Dimerization model of SARS-CoV 3CL^{pro}. When two monomers approach, their domains III initially associate and bring the two chymotrypsin folds together. The two catalytic folds then anchor on each other, probably via the hydrogen bond network between the two helices A′. Based on this scaffold, the two domains III dissociate and rotate. Since the N-fingers are tethered with the last helices of the domains III, they are simultaneously brought to contact with the S1 subsites on the opposite monomers, which might induce the active conformation of the S1 subsites. Finally, the mature dimer would dissociate again due to the dimer–monomer equilibrium of the enzyme in solution.

electron density map (Fig. 6b). At pH 6.0, His163 flipped away from the original position and was trapped between the phenol hydroxyl groups of the two nearby tyrosine residues, Tyr126 and Tyr161; at pH 7.6, it remained the same conformation as in the wild-type structure; while at pH 6.5, both states were present for this residue. Thus, we could conclude that without Phe140 packing, the charging state of His163 might have returned to that of a "normal" and unconstrained histidine residue. We also speculate that the reason why His163 does not flip away in the monomeric structures of SARS-CoV 3CL^{pro}, which were all determined at pH 6.0, is probably because Leu141 has taken the role of Phe140, and Phe140 has pushed Tyr126 away to prevent it from interacting with His163 (Fig. 3b). These observations all demonstrated that Phe140 is the major stabilizing force in maintaining the active conformation of the S1 subsite of SARS-CoV 3CL^{pro}, thus emphasizing again that a properly charged His163 is significant for substrate-binding (Tan et al., 2005).

Implication for dimerization

Remarkably, Ser139 residue does not participate in forming the dimer interfaces of these F140A mutants. Thus, a question has been raised: why does F140A fail to be monomerized? We speculate that this might be because F140A mutation endowed the oxyanion loop with a flexibility large enough to allow it rearrange its interaction with the opposite protomer (*e.g.* the new Asn142…Arg4B H-bond, Fig. 6c), and the dimer stability was compensated to the extent even stronger than that of the wild-type enzyme, as indicated by the smaller retention volume, and thus a larger dimer proportion of F140A in gel filtration compared with the wild-type (Fig. 5). While in S139A structure, the conformational change of the S1 subsite is much more limited due to the presence of Phe140, probably making it difficult for the dimer interface to rearrange. Therefore, the rigidity of the S1 subsite might be another factor contributing to the dimerization of SARS-CoV 3CL^{pro}.

Conclusion

In the current work, we have determined the crystal structures of Ser139_Ala and Phe140_Ala mutants of SARS-CoV 3CL^{pro}. These two mutations are both from the S1 substrate-binding subsite of the enzyme. Ser139 contributes its sidechain hydroxyl in forming three hydrogen bonds with the opposite protomer, and Phe140 donates its mainchain groups to interact with Ser1B from the counterpart N-finger. Interestingly, although these two residues are adjacent, they caused completely different activity loss and structural change of the protease. S139A is monomeric but retains some enzymatic activity, while F140A is still a dimer but inactive. Basically, the whole structure of S139A is very similar to those of the two reported mutation-induced monomeric enzymes. Considering that the positional relationship and the interaction network between domain III and the parental N-finger is essentially unchanged in monomeric and dimeric enzymes, we speculate that during the dimerization process, the rotation of domain III might bring the parental N-finger to contact and activate the S1 subsite of the opposite protomer (Fig. 7). The existence of a small fraction of stable dimer in solution for S139A might account for the remaining activity of this mutant. As for the F140A mutant, the conformational changes observed in crystal structure, especially the pH-dependent flip of His163, have well-reflected the functional roles of Phe140 in both supporting the open conformation of S1 subsite and maintaining the uncharged state of His163 for substrate recognition. Moreover, the deletion of the large aromatic ring of Phe140 might have conferred the oxyanion loop great flexibility so that the dimer interface could be rearranged to restore the stability of the dimer. This might explain why F140A is still a dimer even though Ser139 is absent from its dimer interface. Our work has not only provided the direct structural evidence for the indispensable roles of these two S1 subsite residues in maintaining the dimerization and activity of SARS-CoV 3CL^{pro} but also suggested a plausible dimerization process for the enzyme. More importantly, we showed that the elements involved in dimerization constitute a complex network to cooperatively regulate the activity of the enzyme, a single mutation on the dimer interface could often cause complete dimer dissociation. Our results have strongly supported that targeting the dimerization of SARS-CoV 3CL^{pro} could be an effective strategy for developing inhibitors against this enzyme to combat SARS infection.

Materials and methods

Cloning, expression, purification and gel filtration analysis

The coding sequence of the wild-type 3CL^{pro} was cloned from SARS-CoV Tor2 strain (Sun et al., 2003) and inserted into the BamHI and XhoI sites of the plasmid pGEX4T-1 (Amersham Pharmacia Biotech). Mutations of Ser139_Ala and Phe140_Ala were performed with the QuikChange site-directed mutagenesis kit (Stratagene) using

pGEX4T-1-SARS-CoV 3CL^{pro} as template. The nucleotide sequences of the primers used for single point mutation were:

5′-CATACCATTAAAGGTGCTTTCCTTAATGGATCATGTGG-3′ (forward, S139A)
5′-CCACATGATCCATTAAGGAAAGCACCTTTAATGGTATG-3′ (reverse, S139A)
5′-CATACCATTAAAGGTTCTGCCCTTAATGGATCATGTGG-3′ (forward, F140A)
5′-CCACATGATCCATTAAGGGCAGAACCTTTAATGGTATG-3′ (reverse, F140A).

The resulting plasmids were verified by sequencing and then transformed into *E. coli* BL21 (DE3) cells. The expression and purification protocols for the two mutants are the same as reported in the study of Gly11_Ala mutant (Chen et al., 2008a). In brief, the expression was induced by adding IPTG to 0.5 mM when the A_{600} of the LB medium reached 0.8, and the culture was grown for another 6 h at 25 °C. The recombinant protein was purified in PBS buffer with the Glutathione Sepharose™ 4B affinity column (Amersham Pharmacia Biotech). The GST tag was subsequently cleaved off by thrombin (50 U) at 25 °C for 6 h. The target protein was further purified by MonoQ 10/100 GL column (Amersham Pharmacia Biotech) with a NaCl gradient from 0 to 1.0 M, and dialyzed against 10 mM Tris–HCl pH 7.5, 1 mM EDTA, 5 mM DTT. The gel filtration analysis of S139A mutant is performed in the same buffer at 2 mg/ml, on a HiLoad™ Superdex™ 75 prep grade column (GE Healthcare) at a flow rate of 1 ml/min.

Crystallization and data collection

The two mutants of SARS-CoV 3CL^{pro} were both crystallized at 10 mg/ml by hanging-drop vapor-diffusion method at 4 °C. Crystals of S139A mutant were grown from the mother liquor containing 0.1 M MES pH 6.0, 10% PEG 6000, 1 mM DTT, 5% DMSO. Crystals of F140A were grown at three pH values: 0.1 M MES pH 6.0/0.1 M MES pH 6.5/0.1 M Tris pH 7.6, with 10% PEG 6000, 1 mM DTT and 5% DMSO.

Diffraction data was collected in-house on a Rigaku rotating-anode X-ray generator operated at 100 kV and 100 mA ($\lambda = 1.5418$ Å). Diffraction images were recorded by a Rigaku R-AXIS IV++ imaging-plate detector with an oscillation step of 1°. The crystals were harvested with a nylon loop and flash-cooled in liquid nitrogen. Data collection was performed at 100 K in the cryoprotectant solution containing 30% of glycerol and 70% of the mother liquor. The data sets were indexed, integrated and scaled using the program suite CrystalClear (Rigaku). Statistics of data collection were summarized in Table 1. F140A crystals were difficult to grow at pH 7.6 and their qualities were relatively low, probably because basic pH is unfavorable for the crystallization of SARS-CoV 3CL^{pro} (almost all of its reported crystal structures were obtained at acidic pHs). However, the resultant electron density map was good enough to address our interested problems (*e.g.* the conformation of His163).

Structure determination, refinement and model building

The structures were determined by molecular replacement using Molrep (Vagin and Teplyakov, 1997) of the CCP4 program suite (Collaborative Computational Project, 1994). The protomer (chain A) or the whole dimer in the structure of wild-type SARS-CoV 3CL^{pro} (PDB coed: 1UK4) was used as the search model. Model refinement was initially performed with CNS (Brunger et al., 1998), using standard protocols including simulated annealing, minimization and B-factor refinement. Coot (Emsley and Cowtan, 2004) and refmac5 (Murshudov et al.) were subsequently employed for iterative cycles of model building and refinement. The water molecules were modeled by inspecting the $>3\sigma$ F_o–F_c difference map. The geometry of the model was validated by Procheck (Laskowski et al., 1993). Statistics of the refinement were summarized in Table 1. Note that the average temperature factors are smaller for water molecules than for the

Table 1
Statistics of diffraction data and structure refinement.

	S139A (pH 6.0)	F140A (pH 6.0)	F140A (pH 6.5)	F140A (pH 7.6)
Data collection				
Space group	$P2_12_12_1$	$P2_12_12_1$	$P2_12_12_1$	$P2_12_12_1$
Cell dimensions				
a, *b*, *c* (Å)	90, 90, 90	90, 90, 90	90, 90, 90	90, 90, 90
α, β, γ (°)	34.3, 66.0, 128.2	61.2, 67.9, 149.2	61.2, 68.0, 149.3	61.1, 68.1, 148.9
Resolution (Å)	15.0–2.50 (2.59–2.50)[a]	15.0–2.30 (2.38–2.30)	15.0–2.60 (2.69–2.60)	15.0–2.90 (3.00–2.40)
R_{sym} or R_{merge}[b]	0.135 (0.378)	0.103 (0.327)	0.155 (0.350)	0.189 (0.366)
I/σ	5.4 (2.0)	5.8 (2.1)	4.3 (1.9)	4.9 (1.9)
Completeness (%)	98.7 (99.9)	99.3 (100.0)	95.7 (96.8)	98.4 (99.9)
Redundancy	3.6 (3.8)	3.8 (3.8)	3.4 (3.4)	3.5 (3.6)
Refinement				
Resolution (Å)	15.0–2.50	15.0–2.30	15.0–2.60	15.0–2.90
No. reflections	9981	26699	17902	13355
R_{work}/R_{free}[c]	0.252/0.308	0.208/0.246	0.232/0.306	0.232/0.294
No. atoms	2363	4887	4715	4655
Protein	2309	4628	4604	4634
Water	54	259	111	21
B-factors (Å^2)	36.2	25.9	21.9	22.9
Protein	36.5	25.9	22.1	22.9
Water	22.1	28.1	15.4	5.7
R.M.S. deviations				
Bond lengths (Å)	0.006	0.007	0.006	0.006
Bond angles (°)	0.933	1.057	0.926	0.932
Ramachandran plot (%)				
Most favored	85.3	90.4	86.7	85.6
Allowed	13.6	8.5	11.5	13.3
Generously allowed	0.4	0.6	1.2	0.4
Disallowed	0.8	0.6	0.6	0.8

[a] Values in parentheses are for highest resolution shell.
[b] R_{sym} or $R_{merge} = \sum_h \sum_i |I_{hi} - \langle I_h \rangle| / \sum_h \sum_i I_{hi}$, where I_{hi} and $\langle I_h \rangle$ are the *i*-th and mean measurement of the intensity of reflection *h*, respectively.
[c] R_{work} / $R_{free} = \sum_h F_{o.h} - F_{c.h} / \sum_h F_{o.h}$, where $F_{o.h}$ and $F_{c.h}$ are the observed and calculated structure factor amplitudes, respectively.

polypeptide chain, except for the highest resolution (2.3 Å) structure (F140A, pH 6.0), because in the lower resolution structures, only the most firmly bound water molecules could be detected, the similar phenomenon was also observed in our another structure with low resolution(Yu et al., 2008).

Structural superpositions and RMSD calculations were performed in Pymol. The interfaces between domain III and the parental N-finger were determined by the EBI PISA web server. The figures were all prepared with Pymol (DeLano, 2002). Coordinates and structure factors of the two SARS-CoV $3CL^{pro}$ mutants have been deposited in the Protein Data Bank with accession number of 3F9E for S139A, and 3F9F, 3F9G, and 3F9H for F140A.

Acknowledgments

This work was supported by Sino-European Project on SARS Diagnostics and Antivirals (SEPSDA) (Proposal/Contract no.:003831) and Foundation of Chinese Academy of Sciences (grant KSCX2-YW-R-18).

References

Anand, K., Palm, G.J., Mesters, J.R., Siddell, S.G., Ziebuhr, J., Hilgenfeld, R., 2002. Structure of coronavirus main proteinase reveals combination of a chymotrypsin fold with an extra α-helical domain. EMBO J. 21 (13), 3213.

Anand, K., Ziebuhr, J., Wadhwani, P., Mesters, J.R., Hilgenfeld, R., 2003. Coronavirus main proteinase (3CLpro) structure: basis for design of anti-SARS drugs. Science 300 (5626), 1763–1767.

Bacha, U., Barrila, J., Velazquez-Campoy, A., Leavitt, S.A., Freire, E., 2004. Identification of novel inhibitors of the SARS coronavirus main protease 3CLpro. Biochemistry. (Washington). 43 (17), 4906–4912.

Barretto, N., Jukneliene, D., Ratia, K., Chen, Z., Mesecar, A.D., Baker, S.C., 2005. The papain-like protease of severe acute respiratory syndrome coronavirus has deubiquitinating activity. J. Virol. 79 (24), 15189–15198.

Barretto, N., Jukneliene, D., Ratia, K., Chen, Z., Mesecar, A.D., Baker, S.C., 2006. Deubiquitinating activity of the SARS-CoV papain-like protease. Adv. Exp. Med. Biol. 581, 37–41.

Barrila, J., Bacha, U., Freire, E., 2006. Long-range cooperative interactions modulate dimerization in SARS 3CL pro. Biochemistry 45 (50), 14908–14916.

Brunger, A.T., Adams, P.D., Clore, G.M., DeLano, W.L., Gros, P., Grosse-Kunstleve, R.W., Jiang, J.S., Kuszewski, J., Nilges, M., Pannu, N.S., Read, R.J., Rice, L.M., Simonson, T., Warren, G.L., 1998. Crystallography and NMR system: a new software suite for macromolecular structure determination. Acta. Crystallogr. D. Biol. Crystallogr. 54 (Pt 5), 905–921.

Chang, H.P., Chou, C.Y., Chang, G.G., 2007. Reversible unfolding of the severe acute respiratory syndrome coronavirus main protease in guanidinium chloride. Biophys. J. 92 (4), 1374.

Chen, S., Chen, L., Tan, J., Chen, J., Du, L., Sun, T., Shen, J., Chen, K., Jiang, H., Shen, X., 2005. Severe acute respiratory syndrome coronavirus 3C-like proteinase N terminus is indispensable for proteolytic activity but not for enzyme dimerization. Biochemical and thermodynamic investigation in conjunction with molecular dynamics simulations. J. Biol. Chem. 280 (1), 164–173.

Chen, H., Wei, P., Huang, C., Tan, L., Liu, Y., Lai, L., 2006. Only one protomer is active in the dimer of SARS 3C-like proteinase. J. Biol. Chem. 281 (20), 13894–13898.

Chen, S., Hu, T., Zhang, J., Chen, J., Chen, K., Ding, J., Jiang, H., Shen, X., 2008a. Mutation of Gly-11 on the dimer interface results in the complete crystallographic dimer dissociation of severe acute respiratory syndrome coronavirus 3C-like protease: crystal structure with molecular dynamics simulations. J. Biol. Chem. 283 (1), 554–564.

Chen, S., Zhang, J., Hu, T., Chen, K., Jiang, H., Shen, X., 2008b. Residues on the dimer interface of SARS coronavirus 3C-like protease: dimer stability characterization and enzyme catalytic activity analysis. J. Biochem. 143 (4), 525–536.

Chou, C.Y., Chang, H.C., Hsu, W.C., Lin, T.Z., Lin, C.H., Chang, G.G., 2004. Quaternary structure of the severe acute respiratory syndrome (SARS) coronavirus main protease. Biochemistry 43 (47), 14958–14970.

Collaborative Computational Project, N., 1994. The CCP4 suite: programs for protein crystallography. Acta Crystallogr. D Biol. Crystallogr. 50 (Pt 5), 760–763.

DeLano, W.L., 2002. The PyMOL Molecular Graphics System on World Wide Web. http://www.pymol.org.

Devaraj, S.G., Wang, N., Chen, Z., Tseng, M., Barretto, N., Lin, R., Peters, C.J., Tseng, C.T.K., Baker, S.C., 2007. Regulation of IRF-3-dependent innate immunity by the papain-like protease domain of the severe acute respiratory syndrome coronavirus. J. Biol. Chem. 282 (44), 32208.

Ding, L., Zhang, X.X., Wei, P., Fan, K., Lai, L., 2005. The interaction between severe acute respiratory syndrome coronavirus 3C-like proteinase and a dimeric inhibitor by capillary electrophoresis. Anal. Biochem. 343 (1), 159–165.

Drosten, C., Gunther, S., Preiser, W., van der Werf, S., Brodt, H.R., Becker, S., Rabenau, H., Panning, M., Kolesnikova, L., Fouchier, R.A., Berger, A., Burguiere, A.M., Cinatl, J., Eickmann, M., Escriou, N., Grywna, K., Kramme, S., Manuguerra, J.C., Muller, S., Rickerts, V., Sturmer, M., Vieth, S., Klenk, H.D., Osterhaus, A.D., Schmitz, H., Doerr, H.W., 2003a. Identification of a novel coronavirus in patients with severe acute respiratory syndrome. N. Engl. J. Med. 348 (20), 1967–1976.

Drosten, C., Preiser, W., Gunther, S., Schmitz, H., Doerr, H.W., 2003b. Severe acute respiratory syndrome: identification of the etiological agent. Trends Mol. Med. 9 (8), 325–327.

Emsley, P., Cowtan, K., 2004. Coot: model-building tools for molecular graphics. Acta Crystallogr. D Biol. Crystallogr. 60 (Pt 12 Pt 1), 2126–2132.

Fan, K., Wei, P., Feng, Q., Chen, S., Huang, C., Ma, L., Lai, B., Pei, J., Liu, Y., Chen, J., Lai, L., 2004. Biosynthesis, purification, and substrate specificity of severe acute respiratory syndrome coronavirus 3C-like proteinase. J. Biol. Chem. 279 (3), 1637–1642.

Fouchier, R.A., Hartwig, N.G., Bestebroer, T.M., Niemeyer, B., de Jong, J.C., Simon, J.H., Osterhaus, A.D., 2004. A previously undescribed coronavirus associated with respiratory disease in humans. Proc. Natl. Acad. Sci. U. S. A. 101 (16), 6212–6216.

Graziano, V., McGrath, W.J., DeGruccio, A.M., Dunn, J.J., Mangel, W.F., 2006a. Enzymatic activity of the SARS coronavirus main proteinase dimer. FEBS Lett. 580 (11), 2577–2583.

Graziano, V., McGrath, W.J., Yang, L., Mangel, W.F., 2006b. SARS CoV main proteinase: the monomer–dimer equilibrium dissociation constant. Biochemistry 45 (49), 14632–14641.

Hsu, M.F., Kuo, C.J., Chang, K.T., Chang, H.C., Chou, C.C., Ko, T.P., Shr, H.L., Chang, G.G., Wang, A.H., Liang, P.H., 2005a. Mechanism of the maturation process of SARS-CoV 3CL protease. J. Biol. Chem. 280 (35), 31257–31266.

Hsu, W.C., Chang, H.C., Chou, C.Y., Tsai, P.J., Lin, P.I., Chang, G.G., 2005b. Critical assessment of important regions in the subunit association and catalytic action of the severe acute respiratory syndrome coronavirus main protease. J. Biol. Chem. 280 (24), 22741–22748.

Huang, C., Wei, P., Fan, K., Liu, Y., Lai, L., 2004. 3C-like proteinase from SARS coronavirus catalyzes substrate hydrolysis by a general base mechanism. Biochemistry 43 (15), 4568–4574.

Ksiazek, T.G., Erdman, D., Goldsmith, C.S., Zaki, S.R., Peret, T., Emery, S., Tong, S., Urbani, C., Comer, J.A., Lim, W., Rollin, P.E., Dowell, S.F., Ling, A.E., Humphrey, C.D., Shieh, W.J., Guarner, J., Paddock, C.D., Rota, P., Fields, B., DeRisi, J., Yang, J.Y., Cox, N., Hughes, J.M., LeDuc, J.W., Bellini, W.J., Anderson, L.J., 2003. A novel coronavirus associated with severe acute respiratory syndrome. N. Engl. J. Med. 348 (20), 1953–1966.

Kuo, C.J., Chi, Y.H., Hsu, J.T., Liang, P.H., 2004. Characterization of SARS main protease and inhibitor assay using a fluorogenic substrate. Biochem. Biophys. Res. Commun. 318 (4), 862–867.

Lai, C.C., Jou, M.J., Huang, S.Y., Li, S.W., Wan, L., Tsai, F.J., Lin, C.W., 2007. Proteomic analysis of up-regulated proteins in human promonocyte cells expressing severe acute respiratory syndrome coronavirus 3C-like protease. Proteomics 7 (9), 1446–1460.

Laskowski, R.A., MacArthur, M.W., Moss, D.S., Thornton, J.M., 1993. PROCHECK: a program to check the stereochemical quality of protein structures. J. Appl. Cryst. 26, 283–291.

Lin, C.W., Lin, K.H., Hsieh, T.H., Shiu, S.Y., Li, J.Y., 2006. Severe acute respiratory syndrome coronavirus 3C-like protease-induced apoptosis. FEMS Immunol. Med. Microbiol. 46 (3), 375–380.

Lin, P.I., Chou, C.Y., Chang, H.C., Hsu, W.C., Chang, G.G., 2008. Correlation between dissociation and catalysis of SARS-CoV main protease. Arch. Biochem. Biophys. 472 (1), 34–42.

Lindner, H.A., Fotouhi-Ardakani, N., Lytvyn, V., Lachance, P., Sulea, T., Menard, R., 2005. The papain-like protease from the severe acute respiratory syndrome coronavirus is a deubiquitinating enzyme. J. Virol. 79 (24), 15199–15208.

Lindner, H.A., Lytvyn, V., Qi, H., Lachance, P., Ziomek, E., Menard, R., 2007. Selectivity in ISG15 and ubiquitin recognition by the SARS coronavirus papain-like protease. Arch. Biochem. Biophys. 466 (1), 8–14.

Murshudov, G. N., Vagin, A. A., and Dodson, E. J., Refinement of macromolecular structures by the maximum-likelihood method. Biological Crystallography 907, 4449.

Peiris, J.S., Lai, S.T., Poon, L.L., Guan, Y., Yam, L.Y., Lim, W., Nicholls, J., Yee, W.K., Yan, W.W., Cheung, M.T., Cheng, V.C., Chan, K.H., Tsang, D.N., Yung, R.W., Ng, T.K., Yuen, K.Y., 2003. Coronavirus as a possible cause of severe acute respiratory syndrome. Lancet 361 (9366), 1319–1325.

Ratia, K., Saikatendu, K.S., Santarsiero, B.D., Barretto, N., Baker, S.C., Stevens, R.C., Mesecar, A.D., 2006. Severe acute respiratory syndrome coronavirus papain-like protease: structure of a viral deubiquitinating enzyme. Proc. Natl. Acad. Sci. U. S. A. 103 (15), 5717–5722.

Shi, J., Sivaraman, J., Song, J., 2008. Mechanism for controlling the dimer–monomer switch and coupling dimerization to catalysis of the severe acute respiratory syndrome coronavirus 3C-like protease? J. Virol. 82 (9), 4620–4629.

Shi, J., Song, J., 2006. The catalysis of the SARS 3C-like protease is under extensive regulation by its extra domain. FEBS J. 273 (5), 1035–1045.

Shi, J.H., Wei, Z., Song, J.X., 2004. Dissection study on the SARS 3C-like protease reveals the critical role of the extra domain in dimerization of the enzyme: defining the extra domain as a new target for design of highly-specific protease inhibitors. J. Biol. Chem 279, 24765–24773.

Stockman, L.J., Bellamy, R., Garner, P., 2006. SARS: systematic review of treatment effects. PLoS. Med. 3 (9), e343.

Sulea, T., Lindner, H.A., Purisima, E.O., Menard, R., 2005. Deubiquitination, a new function of the severe acute respiratory syndrome coronavirus papain-like protease? J. Virol. 79 (7), 4550–4551.

Sun, H., Luo, H., Yu, C., Sun, T., Chen, J., Peng, S., Qin, J., Shen, J., Yang, Y., Xie, Y., Chen, K., Wang, Y., Shen, X., Jiang, H., 2003. Molecular cloning, expression, purification, and mass spectrometric characterization of 3C-like protease of SARS coronavirus. Protein Expr. Purif. 32 (2), 302–308.

Tan, J., Verschueren, K.H., Anand, K., Shen, J., Yang, M., Xu, Y., Rao, Z., Bigalke, J., Heisen, B., Mesters, J.R., Chen, K., Shen, X., Jiang, H., Hilgenfeld, R., 2005. pH-dependent conformational flexibility of the SARS-CoV main proteinase (M(pro)) dimer:

molecular dynamics simulations and multiple X-ray structure analyses. J. Mol. Biol. 354 (1), 25–40.
Thiel, V., Ivanov, K.A., Putics, A., Hertzig, T., Schelle, B., Bayer, S., Weissbrich, B., Snijder, E.J., Rabenau, H., Doerr, H.W., Gorbalenya, A.E., Ziebuhr, J., 2003. Mechanisms and enzymes involved in SARS coronavirus genome expression. J. Gen. Virol. 84 (Pt 9), 2305–2315.
Vagin, A., Teplyakov, A., 1997. MOLREP: an automated program for molecular replacement. J. Appl. Cryst. 30, 1022–1025.
Verschueren, K.H.G., Pumpor, K., Anemüller, S., Chen, S., Mesters, J.R., Hilgenfeld, R., 2008. A structural view of the inactivation of the SARS coronavirus main proteinase by benzotriazole esters. Chem. Biol. 15 (6), 597–606.
Yang, H., Yang, M., Ding, Y., Liu, Y., Lou, Z., Zhou, Z., Sun, L., Mo, L., Ye, S., Pang, H., Gao, G. F., Anand, K., Bartlam, M., Hilgenfeld, R., Rao, Z., 2003. The crystal structures of severe acute respiratory syndrome virus main protease and its complex with an inhibitor. Proc. Natl. Acad. Sci. U. S. A. 100 (23), 13190–13195.
Yu, X.L., Hu, T., Du, J.M., Ding, J.P., Yang, X.M., Zhang, J., Yang, B., Shen, X., Zhang, Z., Zhong, W.D., Wen, N., Jiang, H., Zhu, P., Chen, Z.N., 2008. Crystal structure of HAb18G/CD147: implications for immunoglobulin superfamily homophilic adhesion. J. Biol. Chem. 283 (26), 18056–18065.
Zhong, N., Zhang, S., Zou, P., Chen, J., Kang, X., Li, Z., Liang, C., Jin, C., Xia, B., 2008. Without its N-finger, the main protease of severe acute respiratory syndrome coronavirus can form a novel dimer through its C-terminal domain. J. Virol. 82 (9), 4227–4234.
Ziebuhr, J., Heusipp, G., Siddell, S.G., 1997. Biosynthesis, purification, and characterization of the human coronavirus 229E 3C-like proteinase. J. Virol. 71 (5), 3992–3997.
Ziebuhr, J., Snijder, E.J., Gorbalenya, A.E., 2000. Virus-encoded proteinases and proteolytic processing in the Nidovirales. J. Gen. Virol. 81 (Pt 4), 853–879.